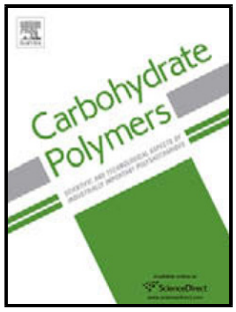

Title: A mechanism for the synergistic gelation properties of gelatin B and xanthan gum aqueous mixtures

Authors: Chang-Sheng Wang, Nick Virgilio, Paula Wood-Adams, Marie-Claude Heuzey

PII: S0144-8617(17)30882-2
DOI: http://dx.doi.org/doi:10.1016/j.carbpol.2017.08.015
Reference: CARP 12622

To appear in:

Received date: 9-5-2017
Accepted date: 3-8-2017

Please cite this article as: Wang, Chang-Sheng., Virgilio, Nick., Wood-Adams, Paula., & Heuzey, Marie-Claude., A mechanism for the synergistic gelation properties of gelatin B and xanthan gum aqueous mixtures.*Carbohydrate Polymers* http://dx.doi.org/10.1016/j.carbpol.2017.08.015

A mechanism for the synergistic gelation properties of gelatin B and xanthan gum aqueous mixtures

Chang-Sheng Wang, [a] *Nick Virgilio,* [a,*] *Paula Wood-Adams,* [b] *Marie-Claude Heuzey* [a,*]

[a] Center for Applied Research on Polymers and Composites (CREPEC), Department of Chemical Engineering, Polytechnique Montréal, Montréal, Québec, H3C 3A7, Canada

[b] CREPEC, Department of Mechanical and Industrial Engineering, Concordia University, Montréal, Québec, H3G 1M8, Canada

* Corresponding authors:

Phone: 1-514-340-4711 #4524 (N. Virgilio); #5930 (M.-C. Heuzey)

Fax: 1-514-340-4159

Email addresses: nick.virgilio@polymtl.ca; marie-claude.heuzey@polymtl.ca

Postal address: Department of Chemical Engineering, Polytechnique Montréal, C.P. 6079 Succursale Centre-Ville, Montréal, Québec, H3C 3A7

ABSTRACT: Gelatin B and xanthan gum aqueous mixtures (GB/XG, (0.2-2%)/0.2% w/v) exhibit enhanced gelling properties compared to their pure component solutions at similar compositions. The mixed gels comprise co-localized networks of GB and XG–rich domains. Our results show that these domains are composed of intermolecular complexes and their aggregates stabilized by the neutralization effect of GB, and linked together by formation of GB triple helices. GB/XG mixtures display composition-dependent microstructural transitions: from discontinuous aggregates (GB/XG ratio ≤ 1) to a continuous GB/XG network (ratio = 2-6), followed by network fragmentation (ratio = 8-10). Increasing the GB Bloom index accelerates network formation and results in higher elastic modulus (*G'*), while increasing the XG molecular weight causes the opposite effect due to diffusion limitations. This work provides a set of fundamental guidelines to design novel thickeners and/or gelling agents based on proteins and polysaccharides, for food or pharmaceutical applications.

KEYWORDS: Gelatin, Xanthan Gum, Gelation Mechanism, Synergy, Rheology, Microstructure

1. Introduction

Proteins and polysaccharides are two of the most important functional biopolymers in food products. Their interactions in aqueous solutions can result in coacervates, complexes or gels depending on charge density, protein/polysaccharide binding affinity and other molecular characteristics (conformation, contour length, chain flexibility and molecular weight) (Turgeon & Laneuville, 2009). These three phase states consequently exhibit different functional properties. For example, protein/polysaccharide coacervates and electrostatic gels can be utilized for ingredient encapsulation (Schmitt & Turgeon, 2011; Turgeon & Laneuville, 2009); complexes and electrostatic gels have excellent texturing properties (Schmitt, Sanchez, Desobry-Banon & Hardy, 1998; Turgeon & Laneuville, 2009); and complexes can provide stabilization due to their interfacial properties (Le, Rioux & Turgeon, 2016; Turgeon & Laneuville, 2009). Protein/polysaccharide electrostatic gels can be formed without heat, enzyme or crosslinking agents, and are therefore promising for the protection of bioactive molecules when used as encapsulation and delivery systems (Le, Rioux & Turgeon, 2016; Turgeon & Laneuville, 2009). In addition, they can be formed at extremely low concentrations of biopolymers (Turgeon & Laneuville, 2009). In order to fully control their functional properties for application design, it is necessary to understand the mechanisms involved in the interactions between proteins and polysaccharides and the way in which these interactions can be tuned (Bernal, Smajda, Smith & Stanley, 1987).

Protein/polysaccharide mixed gel formation depends on the nature and characteristics of the biopolymers. For both proteins (Le, Rioux & Turgeon, 2016) and polysaccharides (Ballester, Turgeon, Sanchez & Paquin, 2005), a higher biopolymer concentration is needed to form a gel when the molecular weight and charge density are lower. Electrostatic forces are the dominant

interactions between proteins and polysaccharides in solution, but other interactions such as hydrogen bonding and hydrophobic interactions can also be involved (Cooper, Dubin, Kayitmazer & Turksen, 2005; Turgeon, Schmitt & Sanchez, 2007). Proteins and polysaccharides can both repel and attract each other even when they carry the same net charge due to the amphiprotic properties of proteins (Seyrek, Dubin, Tribet & Gamble, 2003; van der Wielen, van de Heijning & Brouwer, 2008; Weinbreck, de Vries, Schrooyen & de Kruif, 2003). Electrostatic forces are affected by the protein/polysaccharide ratio, pH, ionic strength and biopolymer charge density (Cooper, Dubin, Kayitmazer & Turksen, 2005; van der Wielen, van de Heijning & Brouwer, 2008).

The gelation properties of protein/polysaccharide electrostatic hydrogels are the result of a delicate balance between repulsive and attractive interactions (van der Wielen, van de Heijning & Brouwer, 2008; Wang, Natale, Virgilio & Heuzey, 2016). Optimal pH, protein/polysaccharide ratio and ionic strength are required to tune their gelation properties. For example, our previous study demonstrated that the highest elastic modulus (*G'*) of a gelatin B (referred to here as L-GB) and XG mixed gel occurs at pH 5.5 (Wang, Natale, Virgilio & Heuzey, 2016). Similarly, β-lactoglobulin/XG and whey protein isolate (WPI)/XG mixtures require an optimum pH and protein to polysaccharide ratio for gelation (Bertrand & Turgeon, 2007; Le & Turgeon, 2013; Sanchez, Schmitt, Babak & Hardy, 1997).

We have also shown that GB/XG aqueous mixtures exhibit time-dependent, pH sensitive synergistic gelation properties (Wang, Natale, Virgilio & Heuzey, 2016). The objective of this work is to investigate the effects of composition, GB Bloom index and XG molecular weight on the rheological properties and microstructure of GB/XG aqueous mixtures, in order to elucidate the mechanism behind the synergistic gelation of this specific protein/polysaccharide pair.

2. Materials and methods

2.1 Materials

Two grades of gelatin (type B), G6650 (Bloom index = 75, Mw = 20-25 kDa, critical gelling concentration $c_{crit} \approx 4.0$ % w/v) (L-GB) and G9382 (Bloom index = 225, Mw = 50 kDa, $c_{crit} \approx 2.0$ % w/v) (H-GB) were purchased from Sigma-Aldrich, Canada. Four grades of xanthan gum (XG) were used: one grade (G1253) was purchased from Sigma-Aldrich Canada (the grade used in our previous work (Wang, Natale, Virgilio & Heuzey, 2016), referred to here as R-XG), while the other three grades with different viscosities (see Figure S1), i.e. Keltrol SF (Low-XG), Keltrol (Med-XG) and Keltrol AP (High-XG), were kindly supplied by CP Kelco U.S., Inc. Other chemicals (HCl, NaOH, Nile Blue A and 5-(4,6-dichlorotriazinyl) aminofluorescein) were of analytical grade (Sigma Aldrich, Canada), and used as received.

2.2 Preparation of GB, XG and GB/XG solutions

GB solutions (0.4-4.0 % w/v) were prepared by allowing GB powder to swell in Milli-Q water (18.2 Ω) for 15-20 min at room temperature, followed by gentle stirring at 60 ^{o}C for 15 min. XG solutions (0.2 and 0.4 % w/v) were prepared by dissolving the powder into Milli-Q water at a magnetic stirring speed of 600-700 rpm for at least 12 h at room temperature. Mixed GB/XG solutions with a fixed XG concentration (0.2 % w/v) and different GB concentrations (0.2-2.0 % w/v) were prepared by mixing equal volumes of GB and XG primary solutions, with magnetic stirring, at 60 ^{o}C for approximately 30 min. The pH of the mixtures was adjusted using 1M HCl or NaOH to the desired values.

2.3 Zeta potential measurements

Zeta potential values of GB and XG solutions were determined by laser doppler velocimetry and phase analysis light scattering (M3-PALS) using a Malvern Zetasizer Nano ZSP instrument

(Malvern Instruments Ltd., Malvern, Worcestershire, UK). The zeta potential was determined from the direction and velocity of the molecules in the applied electric field. The Smoluchowski model was used by the software to convert the electrophoretic mobility measurements into zeta potential values. All the samples were diluted to about 0.05 % (w/v) and then put into a disposable folded capillary cell (DTS1060) to measure the zeta potential. The temperature of the cell was maintained at 25 ^{o}C. The data presented are the average values of three individual measurements.

2.4 "Table-top" rheology

Small volumes (7-8 mL) of freshly prepared GB/XG mixed solutions were transferred into 20 mL vials (Fisherbrand, O.D. × H (with cap): 28 x 61 mm) and kept at room temperature for 24 h. The vials were then inverted to qualitatively assess gel formation and strength.

2.5 Time-resolved small amplitude oscillatory shear

Freshly prepared GB, XG or GB/XG mixed solutions were directly poured into a rough surface Couette flow geometry (cup and bob diameters of 18.066 mm and 16.66 mm, respectively) and measurements were performed using a stress-controlled Physica MCR 501 rheometer (Anton Paar, Graz, Austria). Before the time sweep tests, all systems were heated at a rate of 5 °C/min up to 60 °C. The samples were kept at this temperature for 10 min to erase the previous thermal histories and were subsequently cooled down to 20 °C at a rate of 5 °C/min. Dynamic time sweep measurements were performed at 1 rad/s and 20 °C in the LVE regime (strain = 3 %) for 8 h. The elastic modulus *(G')*, loss modulus (*G"*), and related complex viscosity ($|\eta^*|$) were recorded as functions of time. Samples were covered with a thin film of low viscosity mineral oil to prevent water evaporation. The oil was shown not to affect the rheological measurements. The experiments were performed at least twice with good reproducibility (< 5 %). The results of L-GB solutions

alone in the investigated concentration range (0.2 - 2.0 %, w/v) and of H-GB at concentrations less than 1.0 % w/v were too low and noisy to be reported.

2.6 Confocal laser scanning microscopy (CLSM)

CLSM observations of the GB/XG solutions were performed with an Olympus IX 81 inverted Confocal Microscope (Olympus Canada Inc., Richmond Hill, ON, Canada). GB was stained with Nile Blue A (N0766, Sigma) in solution under magnetic stirring for 30 min before mixing with XG solutions. On the other hand, XG was covalently labeled with 5-(4,6-dichlorotriazinyl) aminofluorescein (DTAF) (D0531, Sigma) using a method described previously (Wang, Natale, Virgilio & Heuzey, 2016). Preliminary experiments showed that labeling did not change the rheological behavior of the solutions. After mixing, solution samples were poured into Petri dishes (P35G-1.5-14-C, MatTek), which were closed with cover slips and hermetically sealed with oil. Observation of XG was made by excitation of DTAF at 488 nm, the emission being recorded between 510 and 550 nm. Observation of GB was made by excitation of Nile Blue A at 633 nm, the emission being recorded between 650 and 680 nm. Micrographs were taken using a 60x objective lens at a 2048 x 2048 pixels resolution. All micrographs were subsequently analyzed using Image J software. To calculate the average size of GB-poor domains, at least 10 small bright regions (50 x 50 μm) from no less than 2 different CLSM images for each sample were selected. Brightness and contrast were adjusted to make GB-poor domains clearer, and the micrographs were then transformed into 8-bit binary images. A median filter was used to remove noise and smooth contours. By modeling GB-poor domains as cylinders, an average diameter value corresponding to a microstructure length scale could be obtained (Esquirol, Sarazin & Virgilio, 2014; Galloway, Montminy & Macosko, 2002; Li & Favis, 2001). The calculation method is briefly described next (Wang, Natale, Virgilio & Heuzey, 2016).

The specific interfacial area, S, between GB-rich domains and GB-poor domains is first given by

$$S = \frac{P}{A} \quad (1)$$

where P is the interfacial perimeter between GB-rich and GB-poor domains (obtained by image analysis), and A is the micrograph area. The average diameter d of GB-poor domains is then obtained as follows:

$$d = \frac{4\Phi_{GB-poor}}{S} \quad (2)$$

where $\Phi_{GB\text{-}poor}$ is the volume fraction of GB-poor domains in solution, also obtained by image analysis (because of microstructure isotropy, the GB-poor domains surface fraction on the micrographs is taken equal to the volume fraction in solution).

In this work, GB-rich domains can also be referred to as biopolymer-rich domains since XG and GB are mixed at pH close to the pI of GB, where strong complexation occurs.

2.7 Micro-differential scanning calorimetry (Micro-DSC)

Micro-DSC experiments were performed on a micro-calorimeter (Microcal Inc., Northampton, MA, US) with a cell volume of 0.520 mL and under an external pressure of 180 kPa. The samples were first degassed using a bath sonicator (FS110, Fisher Scientific, Pittsburgh, PA, US) operated at 135 W for 30 min while heating (final temperature ≈ 80 ^{o}C), and were then injected into the sample cell and kept at 90 ^{o}C for 15 min to remove any effects of thermal history. The samples were subjected to cooling and heating cycles over a temperature range of 10-90 ^{o}C at a rate of 1 ^{o}C/min. The sample cell was cleaned by a continuous flow of hot deionized water after each experiment followed by a water-water baseline test to ensure there was no contamination of the sample cell. The experimental data were analyzed using the Origin-based software provided by

the manufacturer. The transition temperatures were taken at the transition peaks maxima, and the transition enthalpies were determined from the area of the endothermic or exothermic peaks.

3. Results and discussion

3.1 Zeta potential of GB and XG

Figure 1 shows the zeta potential values of all GB and XG grades. The isoelectric point (pI) of L-GB is around 5.2-5.3, which is higher than that of H-GB (≈ 4.9) (**Figure 1a**). The values agree with those reported in the literature (Derkach, Ilyin, Maklakova, Kulichikhin & Malkin, 2015; Williams, Phillips & McKenna, 2003), and both GB grades show positive zeta potential at pH below the pI, while negative values are exhibited above the pI, indicating a change of the overall charge.

Consistent with literature (Le & Turgeon, 2013), the different XG grades show no significant difference in zeta potential values **(Figure 1b**): a strong negative dependency of zeta potential on pH occurs over the range of pH 3.5-5.0. This is due to the deprotonation of -COOH groups with increasing pH, and is followed by a plateau after deprotonation is complete. Note that the data for R-XG were reported in our previous work (Wang, Natale, Virgilio & Heuzey, 2016) .

a)

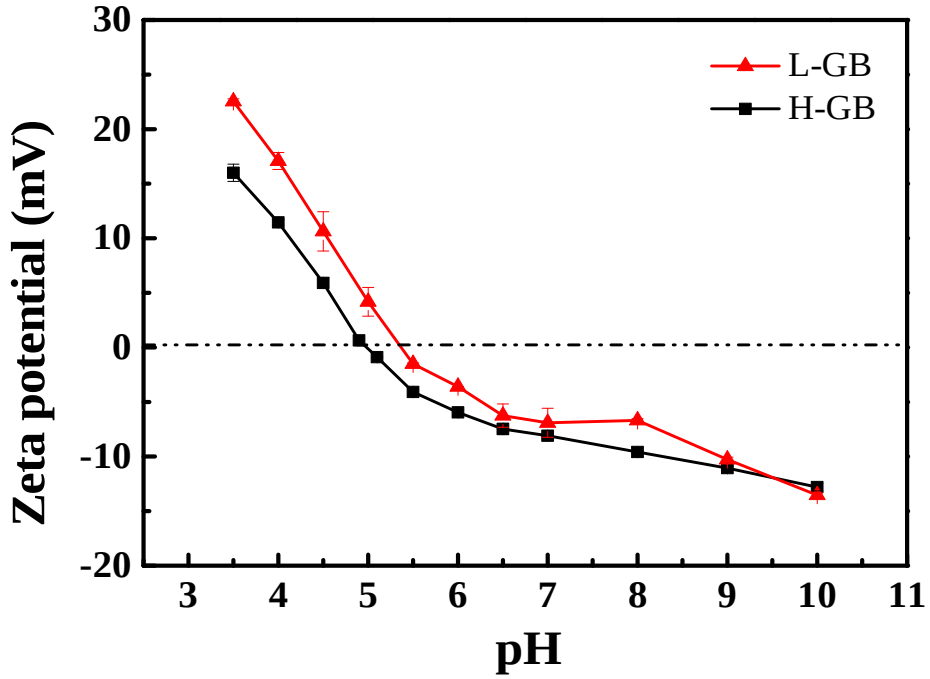

b)

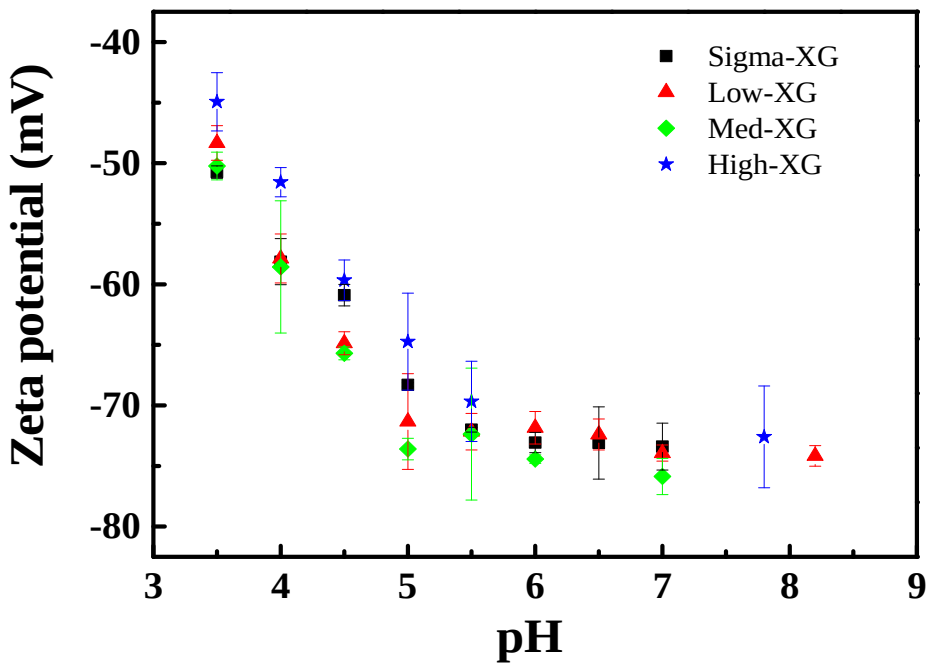

Figure 1. Zeta potential values of the GB (a) and XG (b) grades used in this work.

3.2 "Table-top" rheology

The effects of pH, GB concentration, GB Bloom index and XG molecular weight on the visual aspects of the GB/XG mixed gels are exhibited in **Figure 2**. The properties of GB/XG mixed gels are primarily controlled by a delicate charge balance and are therefore affected by pH and GB concentration. At a given XG concentration, increasing the GB content decreases the charge density of XG due to complexation, which favors the eventual formation of a network. However, the GB content should be carefully controlled to avoid low XG charge densities, which may reduce stability and lead to aggregate formation. For example, L-GB/R-XG mixed gels become more elastic with increasing L-GB concentration and as shown in **Figure 2a**, they exhibit self-supporting properties at L-GB concentrations between 1.0-1.6 % w/v. At 2.0 % w/v L-GB, the system loses its self-holding ability. The decrease in gelation properties is not observed by "table-top" rheology when the GB concentration is close to the critical gelling concentration, as indicated by H-GB/R-XG mixed gels (**Figure 2b**). Here the gels become firmer with increasing H-GB concentration at a given pH.

Similarly, at a pH below the pI of GB, positively charged GB can interact strongly with negatively charged XG. This results in phase separation via the formation of insoluble complexes. At a pH equal to or above the pI of GB, complexation decreases, which makes network formation unlikely. In other words, an optimal pH exists to obtain the strongest gelation properties. For example, see the results for L-GB/R-XG (Wang, Natale, Virgilio & Heuzey, 2016), H-GB/R-XG in **Figure 2b**, and L-GB/Low-, Med-, High-XG mixed gels in **Figure 2c**.

The "table-top" rheology (**Figure 2c**) indicates that the elastic properties decrease with increasing XG molecular weight. These results also show that a synergistic gelation effect occurs

since the critical gelling concentration is much lower for the mixture ($c_{L\text{-}GB}$ = 1.0-1.6 % w/v and $c_{H\text{-}GB} \geq 0.4$ % w/v) than for GB alone ($c_{crit} \approx 4.0$ % w/v for L-GB and $c_{crit} \approx 2.0$ % w/v for H-GB).

a)

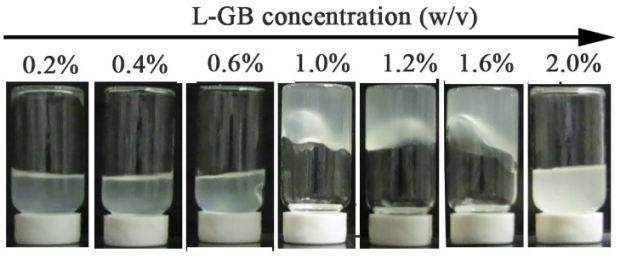

b)

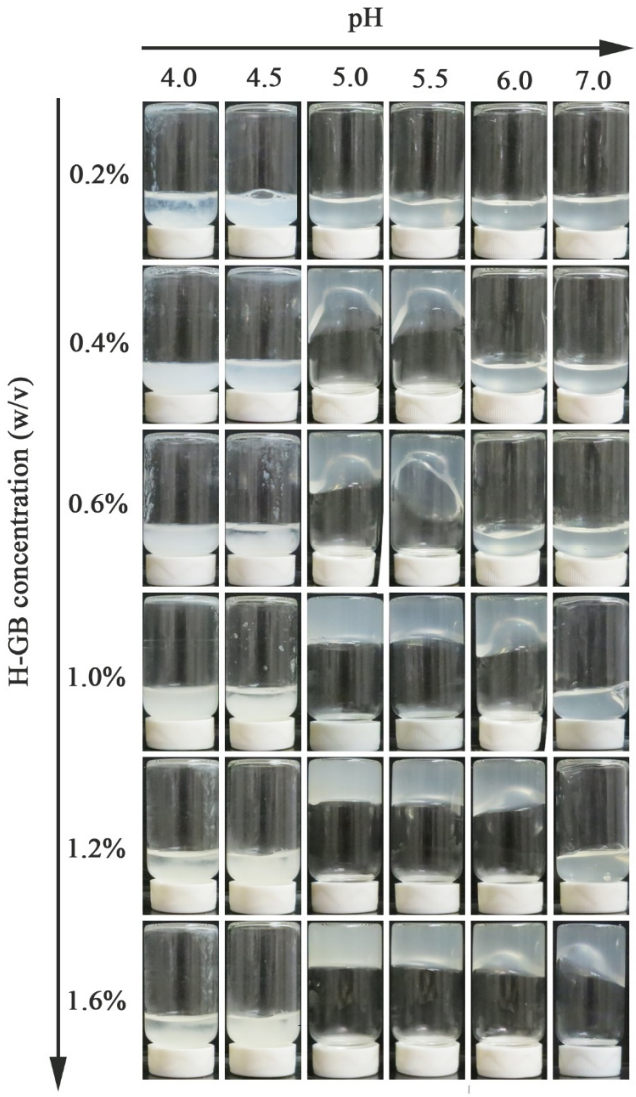

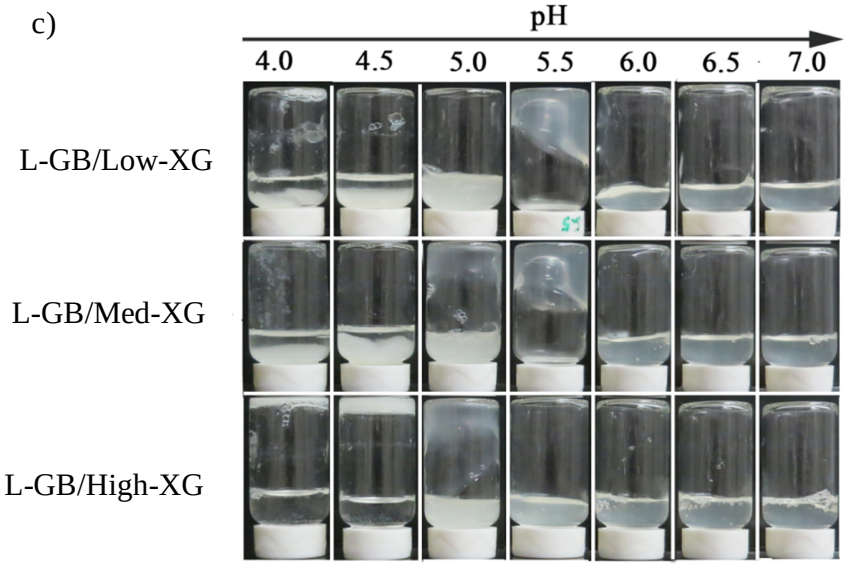

Figure 2. a) Effect of L-GB concentration (c_{GB} = 0.2-2.0 % w/v) on the visual aspect of L-GB/R-XG aqueous mixtures, at pH 5.5; b) effects of pH (4.0-7.0) and H-GB concentration (c_{GB} = 0.2–1.6 % w/v) on the visual aspect of H-GB/R-XG mixtures, H-GB/R-XG ratio = 1-8; c) effects of pH (4.0-7.0) and XG molecular weight on the visual aspect of L-GB/XG mixtures (L-GB:XG ratio = 6, c_{XG} = 0.2 % w/v). The photos were taken after overnight storage.

3.3 Time-resolved small amplitude oscillatory shear

The effects of L-GB concentration and XG molecular weight on the time-dependent rheological properties of GB/XG mixtures were evaluated by dynamic time sweep tests, and the results are presented, respectively, in **Figure 3** and **Figure 4**. The elastic modulus (*G'*) of the XG solution is almost constant in time and always less than the values of the mixtures. The LVE properties of the L-GB solutions are below the resolution limit of our instrument and are therefore not reported. Mixing GB and XG significantly enhances the rheological properties and endows the system with

time-dependent properties. In addition, *G'* is always higher than *G"* for these GB/XG mixtures after 8 hrs (**Figure 3b** and **Figure S2**), showing a soft solid-like behavior.

The *G'* of the mixtures initially increases rapidly followed in most cases by a slow rise, as shown in **Figure 3a**, **Figure 4** and **Figure S2**. The elastic modulus after 8 hrs (G_{8h}') increases significantly for the mixtures containing H-GB as compared to those containing L-GB (compare **Figure 3** and **Figure S2**) but decreases as XG molecular weight increases (**Figure 4**). Note that we observe the inverse effect of XG molecular weight on the initial *G'* (at t = 0 s). The mixtures show a maximum *G'* at a certain GB concentration ($c_{L\text{-}GB}$ = 1.2 % w/v and $c_{H\text{-}GB}$ = 1.6 % w/v) and further increasing the GB content leads to a decrease in gelation properties. These results are coherent with the "table-top" rheology observations presented in §3.2.

a)

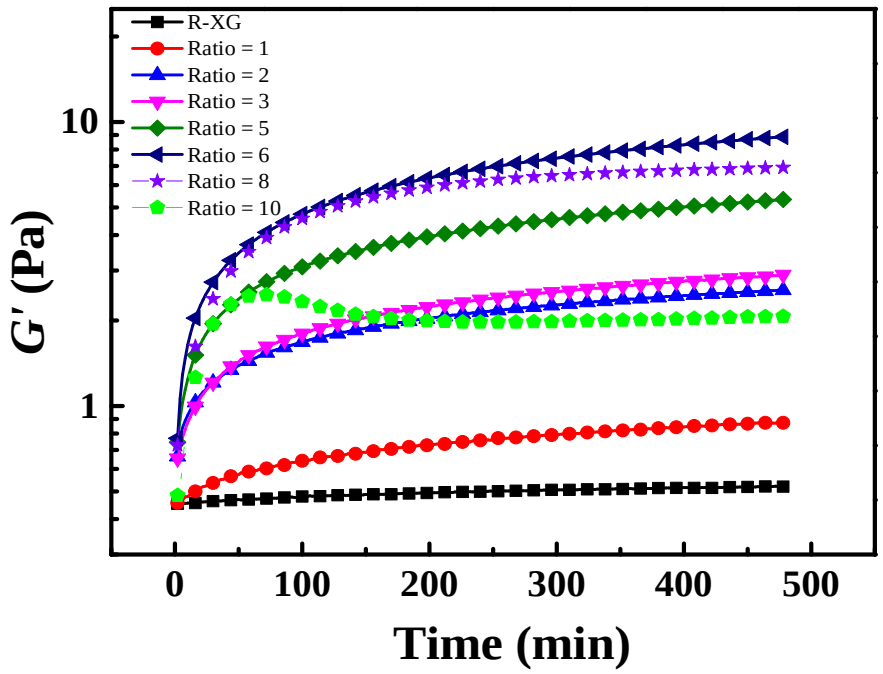

b)

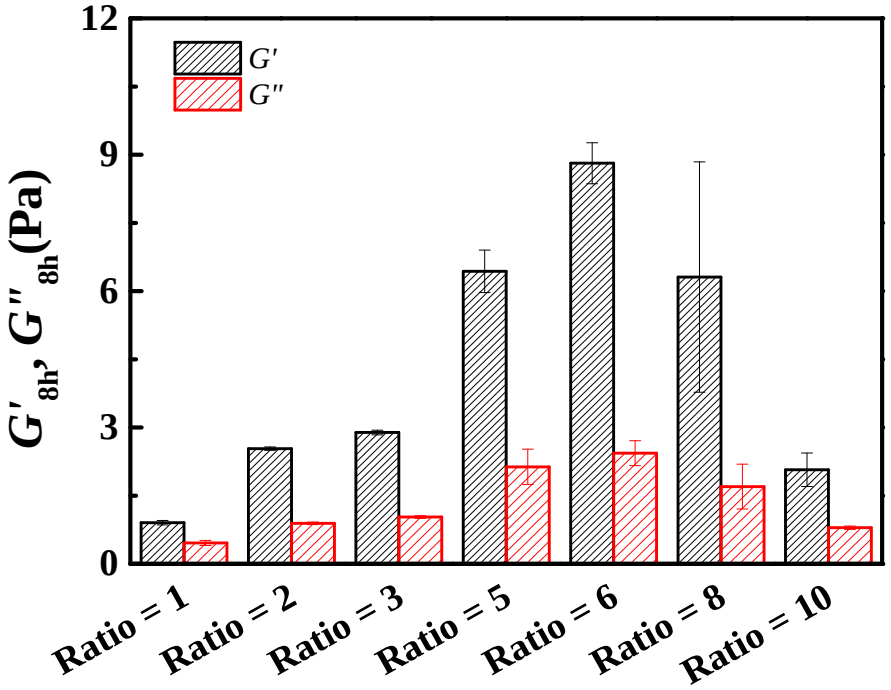

Figure 3. a) Evolution of *G'* as a function of time for the L-GB/R-XG mixtures at ratios (1-10), at pH 5.5; b) *G'* and *G"* after 8 hrs, as a function of L-GB/R-XG ratio. c_{XG} = 0.2 % w/v, ω = 1 rad/s

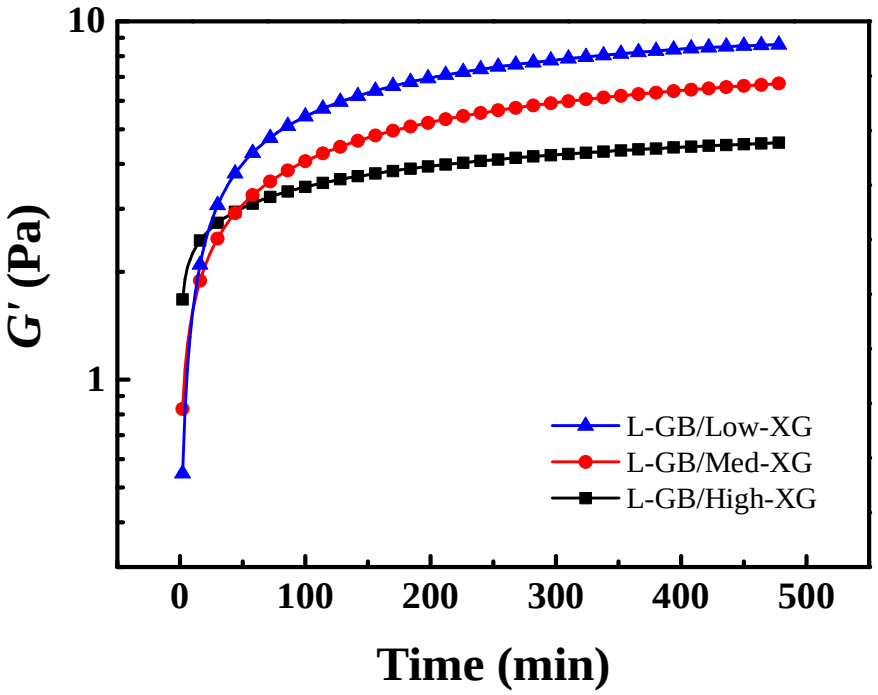

Figure 4. *G'* as a function of time, for the mixtures of L-GB and Low-XG, Med-XG and High-XG respectively, at ratio 6 and pH 5.5. XG concentration = 0.2 % w/v, ω = 1 rad/s.

The ratios of the G_{8h}' of H-GB/R-XG mixtures, to the sum of the G_{8h}' of neat H-GB and R-XG solutions at the concentrations in the corresponding mixtures, were calculated to better evaluate the synergistic effects and are presented in **Figure 5**. This ratio is 22.2 at a GB/XG ratio of 5 (c_{GB} = 1 % w/v and c_{XG} = 0.2 % w/v), and decreases exponentially as GB concentration increases, clearly showing a weakening synergistic effect when the ratio ≥ 5. The H-GB/R-XG mixture even shows a lower G_{8h}' than H-GB alone at ratio GB/XG ratio of 10, showing antagonist or detrimental gelation properties.

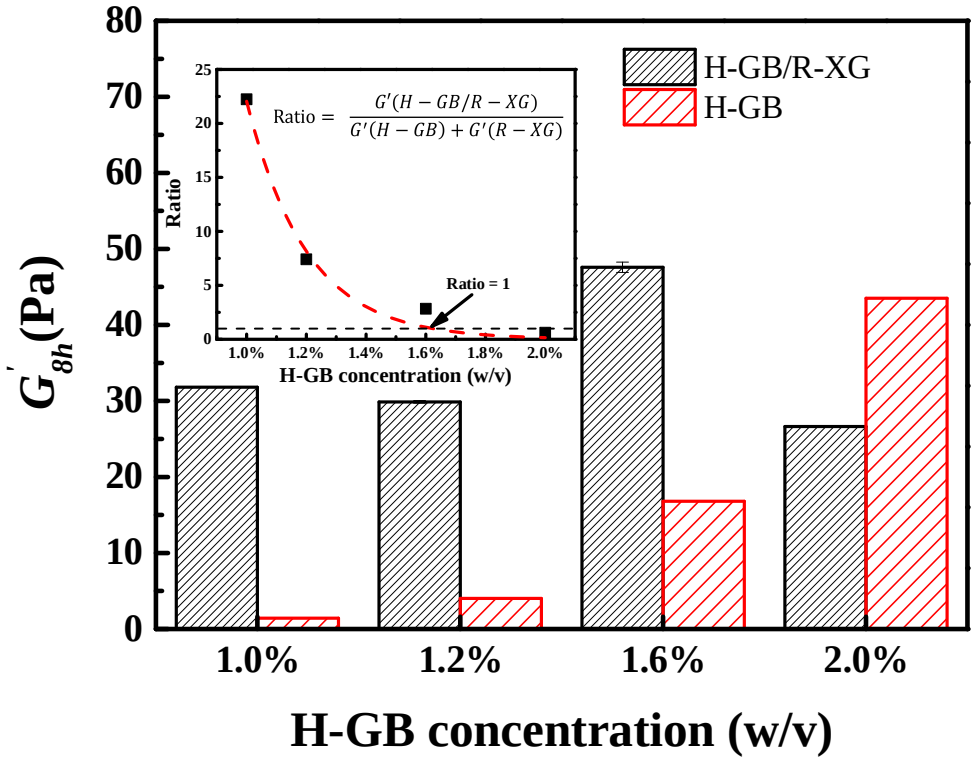

Figure 5. Comparison of G_{8h}' of H-GB solution with and without R-XG after 8 hrs in the rheometer at 20ºC, ω = 1 rad/s, c_{XG} = 0.2 % w/v. The insert shows the ratio of the G_{8h}' of H-GB/R-XG mixtures over the sum of the G_{8h}' of neat H-GB and R-XG at concentrations in the corresponding mixtures, as a function of H-GB concentration.

In the next section, confocal laser scanning microscopy is employed to analyze the microstructure of the mixtures.

3.4 Confocal laser scanning microscopy (CLSM)

Figure 6 shows a set of images for L-GB/Sigma-XG mixtures at different ratios, while **Figure 7** exhibits the effect of XG molecular weight on L-GB microstructure. The microstructure of GB/XG mixed gels generally consists of biopolymer-rich and biopolymer-poor domains. In

comparison, neat GB and XG solutions at similar concentrations have no visible structure and appear homogeneous (images not shown). Both GB and XG exhibit a composition-dependent structural transition in mixed gels. GB has a discontinuous agglomerated morphology at low GB content ($c_{GB} \leq 0.2$ % w/v); a continuous network structure at intermediate GB content followed by a fragmented network structure at high GB content ($c_{L\text{-}GB}$ = 1.6 % w/v and $c_{H\text{-}GB}$ = 2.0 % w/v). This is seen in the left column of **Figure 6**, **Figure 7**, **Figure S4** and **Figure S5**. No XG structure is observed at GB concentrations of 0.2-0.6 % w/v, but a network structure appears when the GB concentration ≥ 1.0 % w/v (middle column of **Figure 6**, **Figure S4**). In this composition range the biopolymer-rich domains consists of GB-rich domains colocalized with XG-rich domains (right column of **Figure 6**, **Figure S4**). For the systems with GB/XG ratios of 5 and 6 we observe significant XG content in the biopolymer-poor domains whereas at higher ratios most of the XG appears to be colocalized with the GB-rich domains. The biopolymer-rich domains first decrease in size (up to ratio 6) and then grow again (ratio ≥ 8) with increasing GB concentration. As we reported previously, the XG network disappears when increasing the pH to 7.0 (**Figure S5**), probably due to the stronger electrostatic repulsion between the molecules (Wang, Natale, Virgilio & Heuzey, 2016).

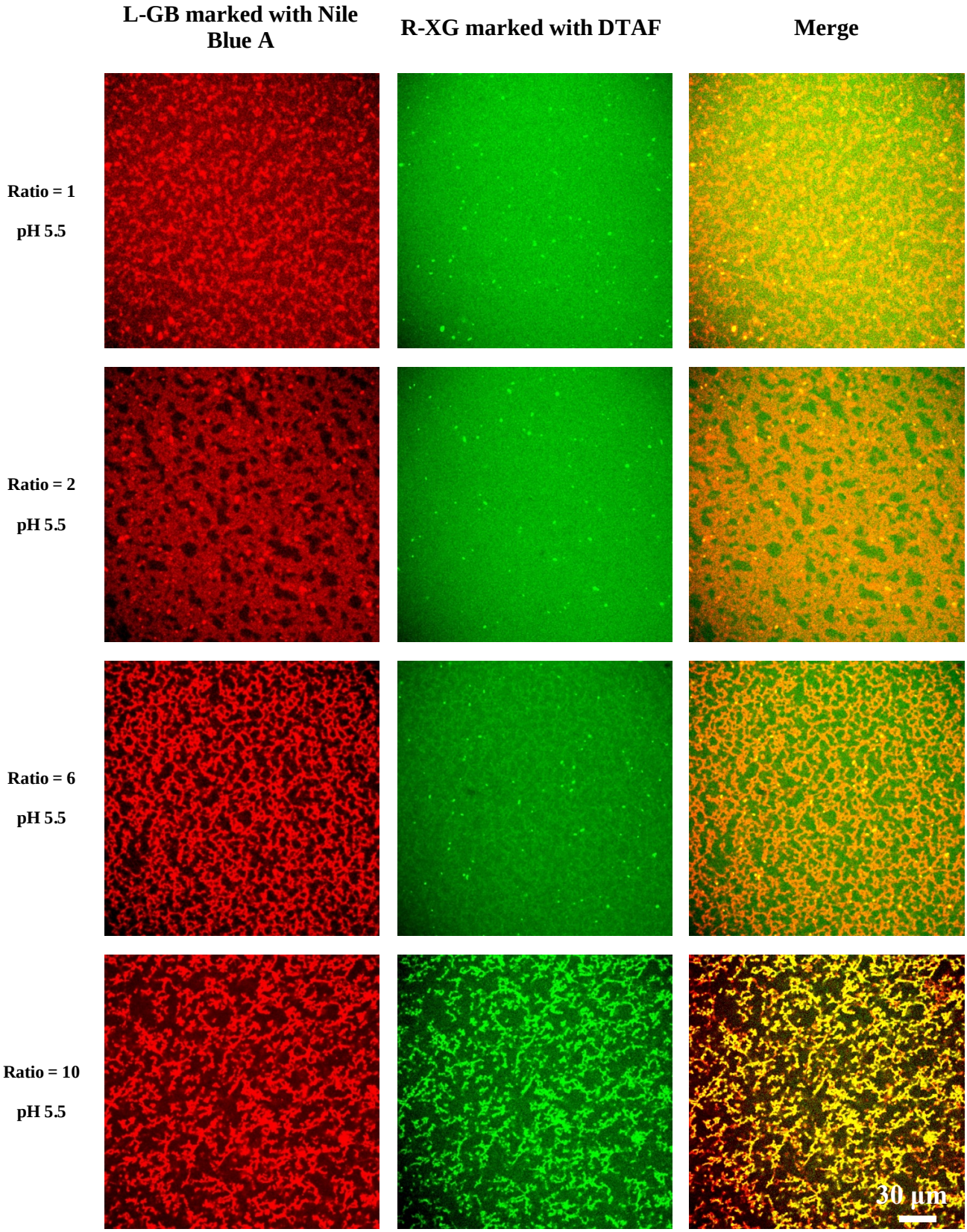

Figure 6. Microstructures of L-GB (red) and R-XG (green) domains in the mixtures at different ratios (1, 2 6 and 10) and merge of the two imaging, at pH 5.5. The images were taken after storage for 24 hrs. Image size: 210 µm x 210 µm.

Increasing GB Bloom index leads to much finer microstructures (compare **Figures 6** and **Figure S5**), whereas increasing XG molecular weight reduces the connectivity of the co-localized networks at ratio 6, finally leading to a granular microstructure (L-GB/High-XG) (**Figure 7**).

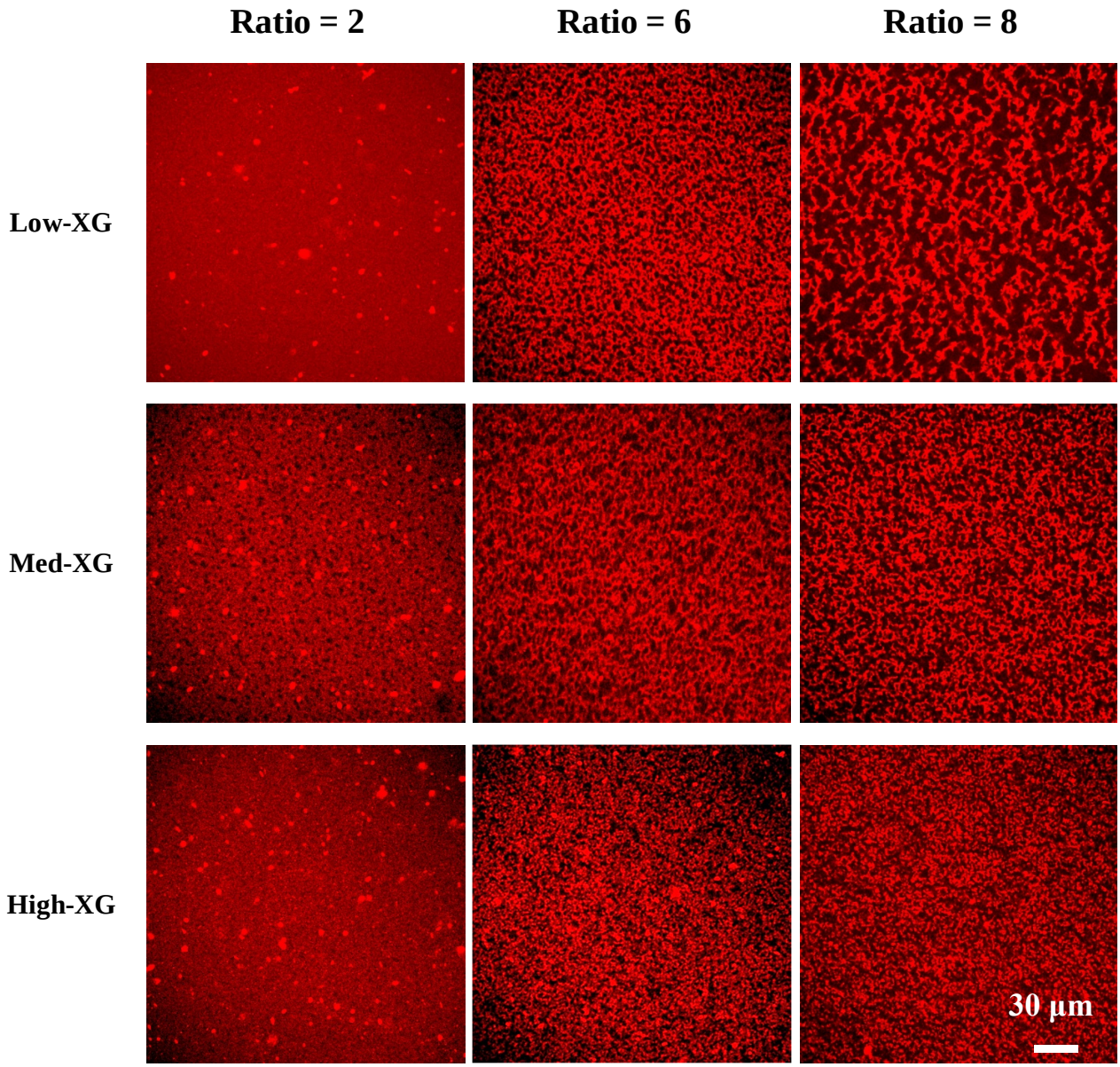

Figure 7. Microstructure of L-GB (red) when mixed with Low-XG, Med-XG and High-XG, respectively, at different ratios (2, 6, and 8) and pH 5.5. The images were taken after storage for 24 hrs at room temperature. Image size: 210 µm x 210 µm.

By modeling biopolymer-poor domains as cylinders, an average diameter value $d_{\text{biopolymer-poor}}$ can be calculated, corresponding to a characteristic microstructural length scale (Esquirol, Sarazin & Virgilio, 2014; Galloway, Montminy & Macosko, 2002; Li & Favis, 2001; Wang, Natale, Virgilio

& Heuzey, 2016). The results are shown in **Figure 8**. The average size of biopolymer-poor domains increases with GB content. The biopolymer-poor domain size is always higher for L-GB/R-XG gels as compared to that of H-GB/R-XG gels.

a)

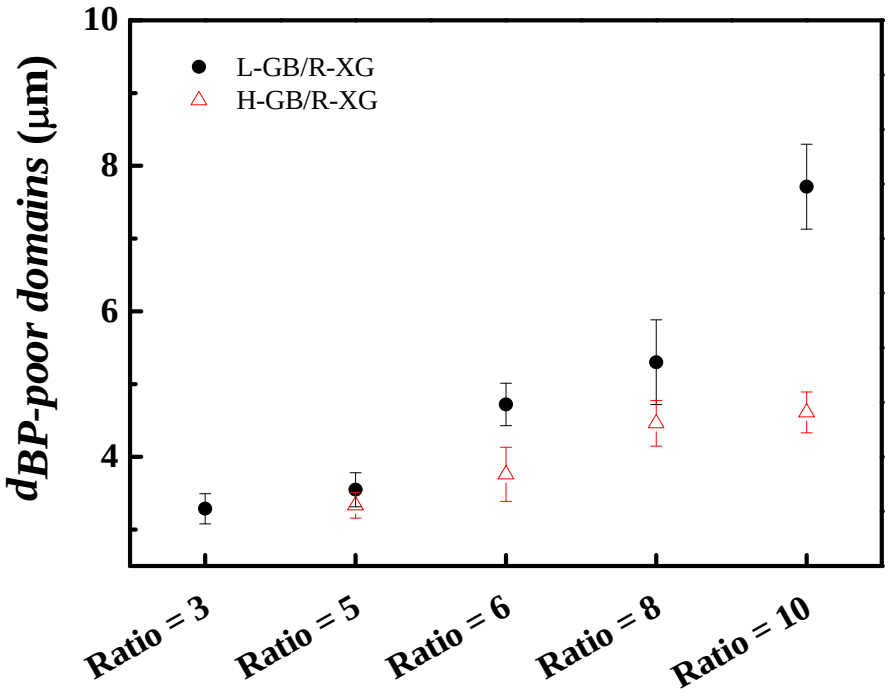

b)

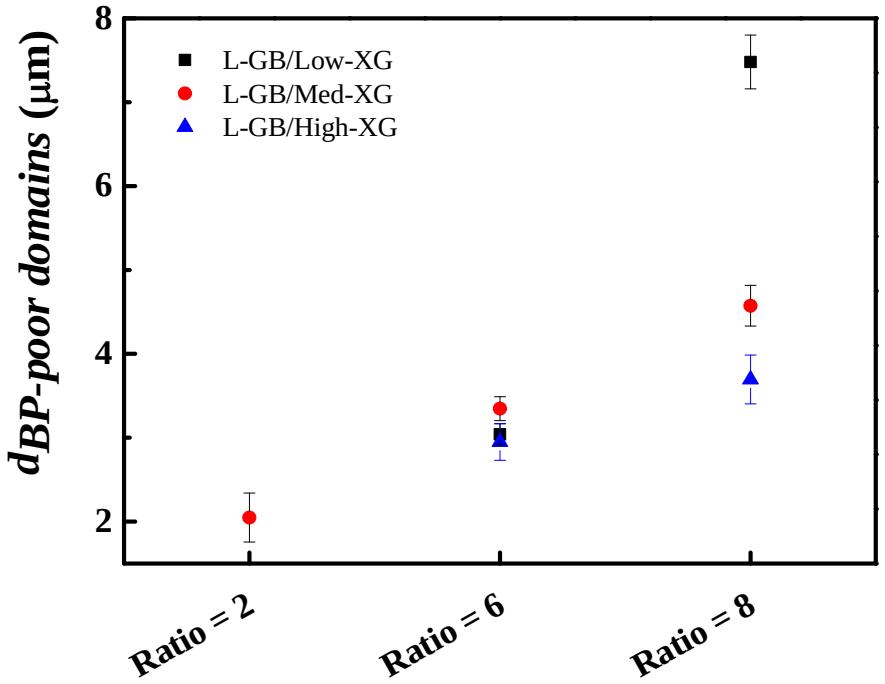

Figure 8. a) Average size of biopolymer-poor (BP-poor) domains in L-GB/R-XG and H-GB/R-XG mixtures, as a function of GB/R-XG ratio; and b) average size of biopolymer-poor domains in L-GB/Low-XG, L-GB/Med-XG and L-GB/High-XG mixtures, as a function of L-GB/XG ratio.

3.5 Micro-calorimetry

Micro-DSC is a powerful technique to study the helix-to-coil (order-to-disorder) transition of polysaccharides and proteins, such as XG (Fitzpatrick, Meadows, Ratcliffe & Williams, 2013; Fitzsimons, Tobin & Morris, 2008; Norton, Goodall, Frangou, Morris & Rees, 1984; Pelletier, Viebke, Meadows & Williams, 2001), DNA (Chiu & Prenner, 2011; Sturtevant, 1987), carrageenan (Liu, Huang & Li, 2016; Liu & Li, 2016) and gelatin (Alqahtani, Ashton, Katopo, Jones & Kasapis, 2016; Sarbon, Badii & Howell, 2015). Here, micro-DSC was used to study the R-XG and L-GB conformation transitions in L-GB/R-XG mixtures, shedding more light on the gelation mechanism.

As shown in **Figure 9**, the R-XG solution at 1.0 % w/v exhibits two peaks located at 35.6 (T_2) and 52.3 ºC (T_3) in the heating cycle. The second peak is consistent with the transition temperatures of 52 ºC observed by Pelletier et al (Pelletier, Viebke, Meadows & Williams, 2001) and ~50 ºC observed by Fitzsimons et. al (Fitzsimons, Tobin & Morris, 2008). This peak is therefore attributed to the XG order-to-disorder (helix-to-coil) transition upon heating (Fitzpatrick, Meadows, Ratcliffe & Williams, 2013; Fitzsimons, Tobin & Morris, 2008; Norton, Goodall, Frangou, Morris & Rees, 1984; Pelletier, Viebke, Meadows & Williams, 2001). The reason for the first peak remains unknown, but it is likely related to impurities in the XG sample, as discussed at the end of this section.

L-GB at 1 % (**Figure 9**) exhibits a peak located at 23.5 ºC attributed to the gelatin helix-to-coil transition (Alqahtani, Ashton, Katopo, Jones & Kasapis, 2016; Sarbon, Badii & Howell, 2015)- (Cheow, Norizah, Kyaw & Howell, 2007).

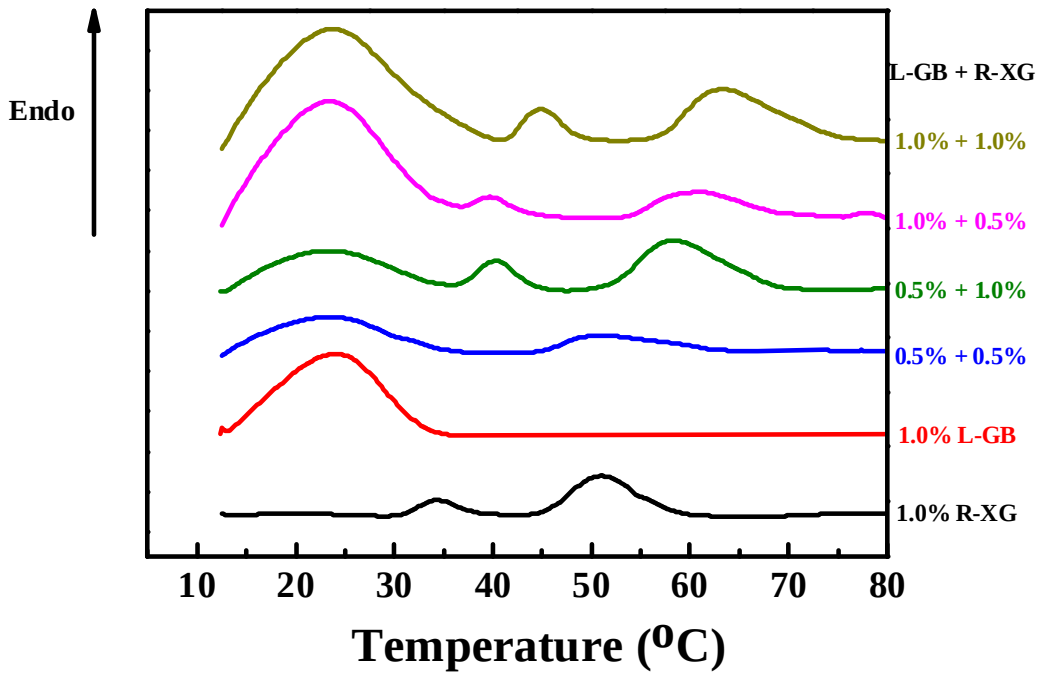

Figure 9. Micro-DSC heating curves, shifted vertically for clarity. Scanning rate = 1 ºC/min.

Table 1. Specific enthalpies and transition temperatures (peak maximum) of L-GB, R-XG and their mixtures during the second micro-DSC heating segment.

			Peak 1		Peak 2		Peak 3	
GB (%)	XG (%)	GB/XG ratio	T_1 (ºC)	ΔH_1^a (J/g)	T_2 (ºC)	ΔH_2^b (J/g)	T_3 (ºC)	ΔH_3^b (J/g)
0.5	1.0	0.5	23.3	5.74	40.3	0.34	58.3	2.66
0.5	0.5	1	23.4	4.91	-	-	51.0	2.06
1.0	1.0	1	23.7	8.64	45.0	1.09	63.3	2.99
1.0	0.5	2	23.4	8.02	39.6	0.82	61.3	2.52
0	1.0	-	-	-	35.6	0.49	52.3	1.54
1.0	0	-	23.5	5.03	-	-	-	-
2.0	0	-	23.6	7.78	-	-	-	-

a: normalized by the mass of GB;
b: normalized by the mass of XG;

The mixtures (**Figure 9**) exhibit three peaks: peak 1 corresponds to L-GB and peak 2 and 3 to R-XG. When R-XG concentration is 1.0 % w/v, the two peaks of the R-XG shift to higher temperatures in the presence of L-GB as compared to those of neat R-XG. The enthalpy of XG also increases with increasing L-GB concentration (**Table 1**). At a XG concentration of 0.5% w/v, peak 2 is no longer visible. These features indicate that more stable XG microstructures are formed with the help of GB. This phenomenon is due to the neutralization of XG molecules after complexation with GB, which then promotes the formation of the XG ordered structure. Furthermore, the enthalpy of L-GB increases in the presence of R-XG. The enthalpy values of 1.0 % w/v L-GB in the mixtures are even higher than that of 2.0 % w/v L-GB alone (**Table 1**). This suggests that XG also enhances or promotes L-GB gelling by triple helix formation.

Note that clarified XG and its mixtures with L-GB were also studied, and they exhibit similar results except that there is only one peak instead of two for the neat clarified XG, and two peaks rather than three for the mixtures (see **Figure S7**).

3.6 Proposed synergistic gelation mechanism

XG molecules are known to undergo a disorder-to-order (coil-to-helix) transition in response to charge screening and/or temperature decrease. The XG backbone takes on a helical conformation and the trisaccharide side chains collapse onto the backbone and stabilize the ordered conformation (Katzbauer, 1998; Rochefort & Middleman, 1987; Stephen, 1995). Weakly associated XG aggregates can subsequently form side-by-side associations between neighboring ordered regions, which gives a tenuous network structure and endows XG dispersions with a weak “gel-like” behavior (Morris, Franklin & I'Anson, 1983; Norton, Goodall, Frangou, Morris & Rees, 1984; Stephen & Phillips, 2010). Based on the properties of XG, the results above and previous observations (Wang, Natale, Virgilio & Heuzey, 2016), a mechanism is proposed to explain the synergistic gelation behavior displayed by GB/XG mixtures (**Figure 10**).

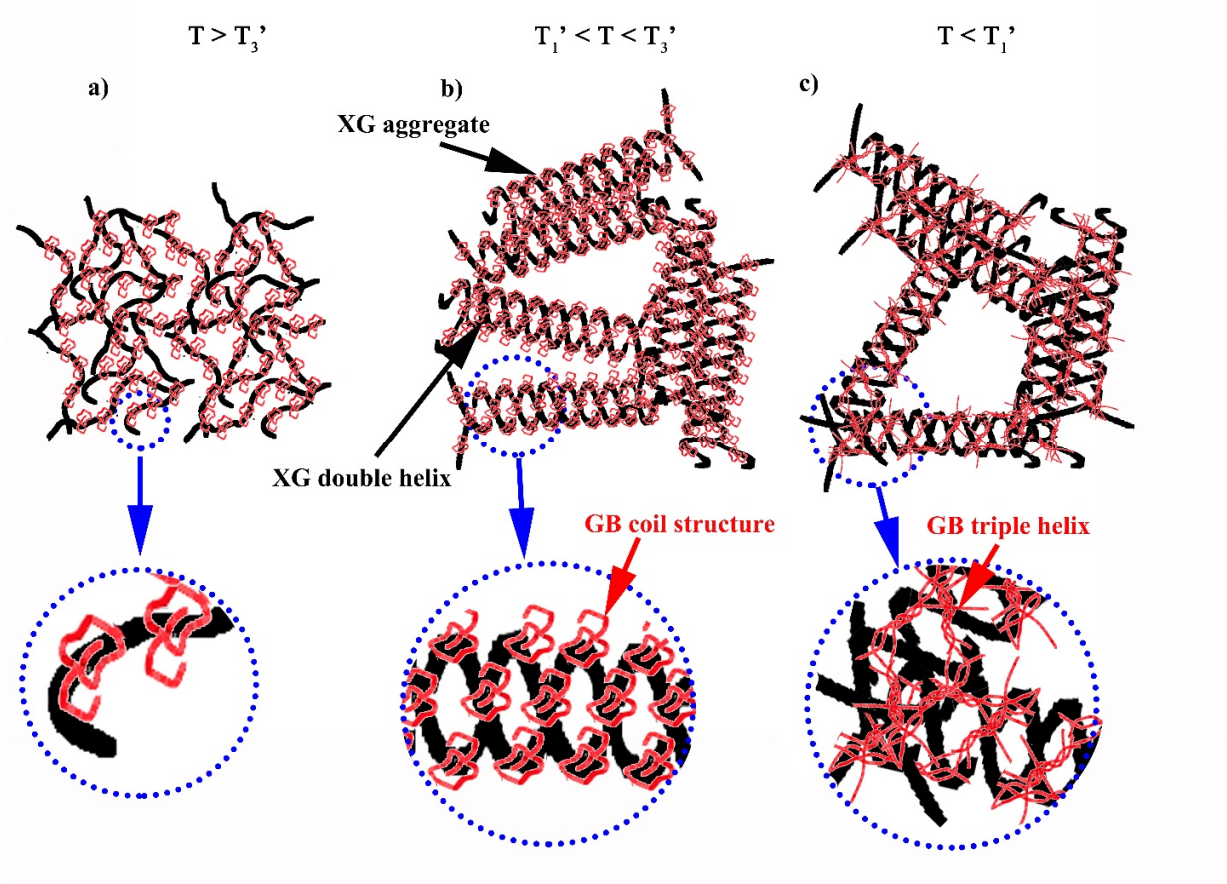

Figure 10. Proposed gelation mechanism in GB/XG mixtures, based on their interactions and molecular conformations.

When mixing the two biopolymers in aqueous solution near the pI of GB, and above the coil-to-helix transition temperature of XG (represented by T_3'), the electrostatic attraction between the negative charges of XG and the positive patches of GB gives rise to soluble GB/XG complexes (**Figure 10a**). This complexation decreases the XG charge density. When the temperature is in-between T_3' and T_1' (representing the coil-to-helix transition of GB), the soluble complexes assemble into interpolymer complexes in the form of XG ordered structures (**Figure 10b**). Since factors that stabilize the ordered structure also favor the formation of XG aggregates (Norton, Goodall, Frangou, Morris & Rees, 1984; Stephen & Phillips, 2010), it is reasonable to say that

large scale assemblies of interpolymer complexes stabilized by GB are also formed under these conditions through side-by-side associations between the ordered XG domains. The local concentrations of both GB and XG are therefore increased. When the system is cooled down below T_1', GB triple helix formation occurs, promoted by its enhanced local concentration. With time, GB/XG interpolymer complexes and aggregates concentrate locally in space and become linked together due to GB gelling (**Figure 10c**). This finally results in a percolated network of biopolymer-rich domains, explaining the observed increase in *G'* of GB/XG mixtures with time (**Figure 3**, **Figure 4** and **Figure S2**). When the network is heated again, the system first goes through the helix-to-coil transition of GB (T_1 in **Table 1**), then through the helix-to-coil transition of XG (T_3 in **Table 1**), since the process is reversible.

The proposed mechanism is further supported by a rheological temperature sweep (**Figure 11**). Starting at 20 °C, when the temperature increases, we can clearly observe the helix-to-coil transition in the 4.0 % L-GB system at ~25 °C, while no such features are evident in the case of 0.2 % w/v R-XG due to the low concentration. However, we do see the helix-to-coil transition at around 52 ^{o}C if the R-XG concentration is increased to 1 % w/v (**Figure S8**), which is consistent with the micro-DSC results (**Figure 9** and **Table 1**). For the mixture, we observe the helix-to-coil transition of the GB at just above 25 °C with the characteristic drop in the *G'*. This demonstrates that the viscoelastic properties of the GB/XG gels, are mainly the result of the GB network up to about 30 °C.

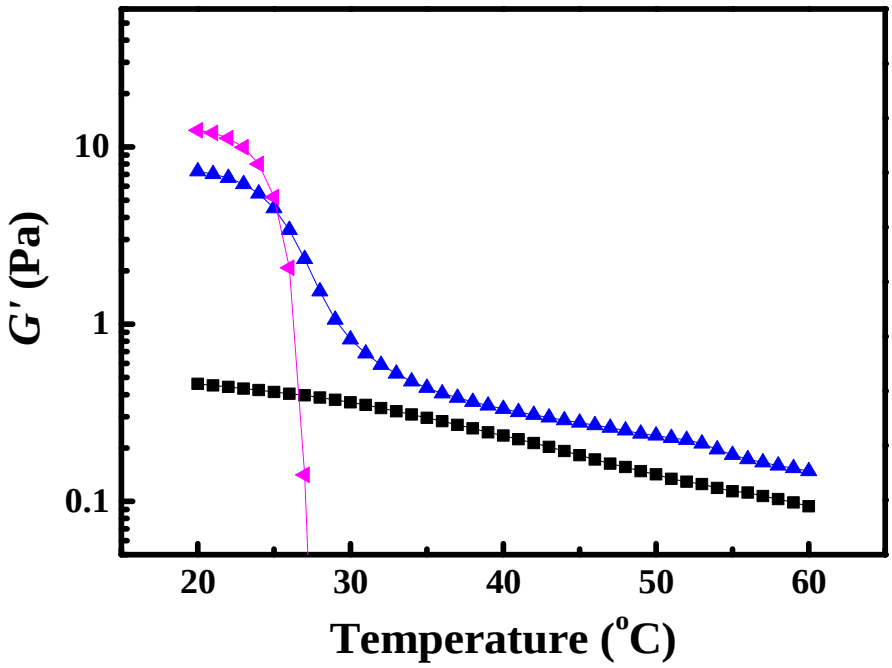

Figure 11. Evolution of *G'* during heating of three systems: (◯) L-GB = 4.0 % w/v, (◯) L-GB/R-XG = 6, total concentration = 1.4 % w/v and (■) R-XG 0.2 % w/v. Heating rate: 0.2 °C/min

4 Conclusion

A gelation mechanism is proposed for gelatin B (GB)/xanthan gum (XG) aqueous mixtures. Soluble GB/XG complexes form near the isoelectric point of GB, above the coil-to-helix transition temperature of XG, followed by a disorder-to-order transition of XG due to the GB neutralization effect when the temperature is in-between the coil-to-helix transition temperature of XG and GB. The two biopolymers are locally concentrated due to the formation of large scale assemblies of interpolymer complexes stabilized by GB, and once cooled below the transition temperature of GB, a network composed of biopolymer-rich domains forms and develops over time. Increasing

GB concentration favors the disorder-to-order transition of XG by decreasing its charge density - however, too low XG charge density destabilizes the system and results in aggregation. Therefore, the GB/XG ratio must be carefully controlled to maintain the network structure and the gelation properties. Stronger interactions between GB/XG interpolymer complexes when cooling down leads to a faster initial evolution and higher *G'*, as well as a denser network. Increasing the XG molecular weight decreases the mobility of soluble and/or interpolymer complexes, which then weakens the concentrating effect and resulting gel properties. We are now currently investigating if this mechanism applies to other protein/polysaccharide systems. This work brings a fundamental understanding to the effects of proteins and polysaccharides interactions in solutions, and provides important guidelines to design novel thickeners and/or gelling agents, encapsulation and delivery systems.

Supporting Information: additional rheological results, confocal microscopy observations and micro-DSC characterization.

Acknowledgements

The authors thank the Natural Sciences and Engineering Research Council of Canada (NSERC) and CREPEC for financial support, and the China Scholarship Council (CSC) for providing a scholarship to Mr. Wang. The authors also acknowledge Dr. Nicolas Tran-Khanh from Polytechnique Montreal for performing the CLSM observations, Dr. Françoise M. Winnik from University of Montreal for allowing us to use micro-DSC, Dr. Evgeniya Korchagina from University of Montreal for her help using micro-DSC and useful discussions, Ms Helia Sojoudiasli from Polytechnique Montreal for useful discussions and Dr. Ross Clark from CP Kelco U.S., Inc for providing the XG samples.

References

Alqahtani, N. K., Ashton, J., Katopo, L., Jones, O. A. H., & Kasapis, S. (2016). Effect of Oat Particle Concentration and Size Distribution on the Phase Behaviour of Mixtures with Gelatin. *Journal of Food and Nutrition Research, 4*(2), 69-75.

Ballester, S. I. L., Turgeon, S. L., Sanchez, C., & Paquin, P. (2005). Gelation of Undenatured Proteins with Polysaccharides. Google Patents.

Bernal, V. M., Smajda, C. H., Smith, J. L., & Stanley, D. W. (1987). Interactions in Protein/Polysaccharide/Calcium Gels. *Journal of Food Science, 52*(5), 1121-1125.

Bertrand, M.-E., & Turgeon, S. L. (2007). Improved gelling properties of whey protein isolate by addition of xanthan gum. *Food Hydrocolloids, 21*(2), 159-166.

Cheow, C. S., Norizah, M. S., Kyaw, Z. Y., & Howell, N. K. (2007). Preparation and characterisation of gelatins from the skins of sin croaker (Johnius dussumieri) and shortfin scad (Decapterus macrosoma). *Food Chemistry, 101*(1), 386-391.

Chiu, M. H., & Prenner, E. J. (2011). Differential scanning calorimetry: An invaluable tool for a detailed thermodynamic characterization of macromolecules and their interactions. *Journal of Pharmacy and Bioallied Sciences, 3*(1), 39-59.

Cooper, C., Dubin, P., Kayitmazer, A., & Turksen, S. (2005). Polyelectrolyte–protein complexes. *Current Opinion in Colloid & Interface Science, 10*(1), 52-78.

Derkach, S. R., Ilyin, S. O., Maklakova, A. A., Kulichikhin, V. G., & Malkin, A. Y. (2015). The rheology of gelatin hydrogels modified by κ-carrageenan. *LWT-Food Science and Technology, 63*(1), 612-619.

Esquirol, A.-L., Sarazin, P., & Virgilio, N. (2014). Tunable Porous Hydrogels from Cocontinuous Polymer Blends. *Macromolecules, 47*(9), 3068-3075.

Fitzpatrick, P., Meadows, J., Ratcliffe, I., & Williams, P. A. (2013). Control of the properties of xanthan/glucomannan mixed gels by varying xanthan fine structure. *Carbohydrate Polymers, 92*(2), 1018-1025.

Fitzsimons, S. M., Tobin, J. T., & Morris, E. R. (2008). Synergistic binding of konjac glucomannan to xanthan on mixing at room temperature. *Food Hydrocolloids, 22*(1), 36-46.

Galloway, J. A., Montminy, M. D., & Macosko, C. W. (2002). Image analysis for interfacial area and cocontinuity detection in polymer blends. *Polymer, 43*(17), 4715-4722.

Katzbauer, B. (1998). Properties and applications of xanthan gum. *Polymer Degradation and Stability, 59*(1), 81-84.

Le, X. T., Rioux, L.-E., & Turgeon, S. L. (2016). Formation and functional properties of protein-polysaccharide electrostatic hydrogels in comparison to protein or polysaccharide hydrogels. *Advances in Colloid and Interface Science*.

Le, X. T., & Turgeon, S. L. (2013). Rheological and structural study of electrostatic cross-linked xanthan gum hydrogels induced by [small beta]-lactoglobulin. *Soft Matter, 9*(11), 3063-3073.

Li, J., & Favis, B. (2001). Characterizing co-continuous high density polyethylene/polystyrene blends. *Polymer, 42*(11), 5047-5053.

Liu, S., Huang, S., & Li, L. (2016). Thermoreversible gelation and viscoelasticity of κ-carrageenan hydrogels. *Journal of Rheology (1978-present), 60*(2), 203-214.

Liu, S., & Li, L. (2016). Thermoreversible gelation and scaling behavior of Ca 2+-induced κ-carrageenan hydrogels. *Food Hydrocolloids, 61*, 793-800.

Morris, V. J., Franklin, D., & I'Anson, K. (1983). Rheology and microstructure of dispersions and solutions of the microbial polysaccharide from Xanthomonas campestris (xanthan gum). *Carbohydrate research, 121*, 13-30.

Norton, I. T., Goodall, D. M., Frangou, S. A., Morris, E. R., & Rees, D. A. (1984). Mechanism and dynamics of conformational ordering in xanthan polysaccharide. *Journal of Molecular Biology, 175*(3), 371-394.

Pelletier, E., Viebke, C., Meadows, J., & Williams, P. (2001). A rheological study of the order–disorder conformational transition of xanthan gum. *Biopolymers, 59*(5), 339-346.

Rochefort, W. E., & Middleman, S. (1987). Rheology of Xanthan Gum: Salt, Temperature, and Strain Effects in Oscillatory and Steady Shear Experiments. *Journal of Rheology, 31*(4), 337-369.

Sanchez, C., Schmitt, C., Babak, V. G., & Hardy, J. (1997). Rheology of whey protein isolate-xanthan mixed solutions and gels. Effect of pH and xanthan concentration. *Food / Nahrung, 41*(6), 336-343.

Sarbon, N. M., Badii, F., & Howell, N. K. (2015). The effect of chicken skin gelatin and whey protein interactions on rheological and thermal properties. *Food Hydrocolloids, 45*, 83-92.

Schmitt, C., Sanchez, C., Desobry-Banon, S., & Hardy, J. (1998). Structure and Technofunctional Properties of Protein-Polysaccharide Complexes: A Review. *Critical Reviews in Food Science and Nutrition, 38*(8), 689-753.

Schmitt, C., & Turgeon, S. L. (2011). Protein/polysaccharide complexes and coacervates in food systems. *Advances in Colloid and Interface Science, 167*(1–2), 63-70.

Seyrek, E., Dubin, P. L., Tribet, C., & Gamble, E. A. (2003). Ionic strength dependence of protein-polyelectrolyte interactions. *Biomacromolecules, 4*(2), 273-282.

Stephen, A. M. (1995). *Food polysaccharides and their applications*. CRC Press.

Stephen, A. M., & Phillips, G. O. (2010). *Food polysaccharides and their applications.* CRC Press.

Sturtevant, J. M. (1987). Biochemical Applications of Differential Scanning Calorimetry. *Annual Review of Physical Chemistry, 38*(1), 463-488.

Turgeon, S. L., & Laneuville, S. I. (2009). CHAPTER 11 - Protein + Polysaccharide Coacervates and Complexes: From Scientific Background to their Application as Functional Ingredients in Food Products A2 - Kasapis, Stefan. In I. T. Norton & J. B. Ubbink (Eds.). *Modern Biopolymer Science* (pp. 327-363). San Diego: Academic Press.

Turgeon, S. L., Schmitt, C., & Sanchez, C. (2007). Protein–polysaccharide complexes and coacervates. *Current Opinion in Colloid & Interface Science, 12*(4–5), 166-178.

van der Wielen, M. W. J., van de Heijning, W., & Brouwer, Y. (2008). Cellulose Gum as Protective Colloid in the Stabilization of Acidified Protien Drinks. In P. A. Williams & G. O. Phillips (Eds.). *Gums and Stabilisers for the Food Industry 14* (pp. 495-502). London, UK: The Royal Society of Chemistry.

Wang, C.-S., Natale, G., Virgilio, N., & Heuzey, M.-C. (2016). Synergistic gelation of gelatin B with xanthan gum. *Food Hydrocolloids, 60*, 374-383.

Weinbreck, F., de Vries, R., Schrooyen, P., & de Kruif, C. G. (2003). Complex Coacervation of Whey Proteins and Gum Arabic. *Biomacromolecules, 4*(2), 293-303.

Williams, P., Phillips, G., & McKenna, B. (2003). The use of hydrocolloids to improve food texture. *Texture in food. Volume 1: Semi-solid foods*, 251-274.